J Mater Sci: Mater Med (2010) 21:419–429
DOI 10.1007/s10856-009-3883-1

Low temperature preparation of calcium phosphate structure via phosphorization of 3D-printed calcium sulfate hemihydrate based material

J. Suwanprateeb · W. Suvannapruk · K. Wasoontararat

Received: 14 July 2009 / Accepted: 17 September 2009 / Published online: 26 September 2009

Abstract The conversion of newly developed three dimensionally printed calcium sulfate hemihydrate (70–90% wt/wt $CaSO_4 \cdot 0.5 \cdot H_2O$) based materials to calcium phosphate bioceramics by phosphorization in di-sodium hydrogen phosphate solution at 80°C for 4, 8, 16 and 24 h was studied. It was found that transformation rate, phase composition and mechanical properties were influenced by porosity in the fabricated samples and by the duration of the phosphorization treatment. Formulation with 85% $CaSO_4 \cdot 0.5\ H_2O$ showed the fastest transformation rate and resulted in the highest flexural modulus and strength. Depending on the materials formulation, XRD, FT-IR and EDS revealed that calcium deficient hydroxyapatite (CDHA) or a mixture of CDHA and dicalcium phosphate anhydrous (DCPA) were the resulting phases in the transformed samples. After cell culturing for 14 and 21 days, human osteoblast cells were observed to attach to and attain normal morphology on the surface of the transformed sample containing 85% $CaSO_4 \cdot 0.5\ H_2O$. Various sizes and shapes of mineralized nodules were also found after 21 days.

1 Introduction

Recently, three-dimensional printing (3DP) has been investigated as a new tool to construct three dimensional calcium phosphate scaffolds since it can provide sufficient control over both architecture and macro- and microporosity. This process normally involves a high temperature sintering step to burn out the binders and to strengthen the structure [1–9]. Although this high temperature sintered calcium phosphate has been used as tissue-engineered bone repair scaffold due to its good osteoconductivity, the resorption rate is very low due to its high crystallinity [10, 11]. In addition, high shrinkage was also encountered which required the addition of a size compensation factor during the designing step in order to achieve correct dimensions of the final structure. Alternatively, low temperature routes have been studied to produce 3DP calcium phosphate scaffolds of low crystalline hydroxyapatite, dicalcium phosphate dihydrate (DCPD also known as brushite), dicalcium phosphate anhydrous (DCPA or monetite), tricalcium phosphate, calcium pyrophosphate and tetracalcium phosphate that degrade more quickly [12–16]. These low temperature calcium phosphates are expected to show both osteoconductivity and osteclastic resorbability in vivo. In the case of low crystalline hydroxyapatite, low temperature phase transformation from gypsum by phosphate solution was one of techniques that have been studied since it is a relatively simple process [17–19]. This technique was also employed to transform 3DP material fabricated using commercially available raw material to hydroxyapatite [20]. However, the colour of the converted structure changed from white to dark brown and it was fragile; as a result it was not suitable for medical application, hence further improvement is still needed.

In this study, phosphorization of newly formulated 3DP samples based on calcium sulfate hemihydrates was carried out to produce poorly crystalline hydroxyapatite samples with the aim of preventing the above mentioned drawbacks. Physical and mechanical properties of as-fabricated 3DP material, solution treated 3DP material and traditional

J. Suwanprateeb (✉) · W. Suvannapruk · K. Wasoontararat
National Metal and Materials Technology Center, National Science and Technology Development Agency, Ministry of Science and Technology, 114 Paholyothin Road, Klong 1, Pathumthani 12120, Klongluang, Thailand
e-mail: jintamai@mtec.or.th

molded calcium sulfate hemihydrate were compared to study the influences of processing parameters including materials composition and soaking periods. Cell culture of selected representative specimens was also carried out to ensure the biocompatibility of the developed material.

2 Materials and methods

2.1 Materials

Raw materials used in this study were calcium sulfate hemihydrate (Lafarge Prestia Co., Ltd, Thailand) and pre-gelatinized starch (Thaiwah Co., Ltd, Thailand). These materials were supplied in the form of powders and used without further sieving.

2.2 Specimen preparation

The raw material mixture was prepared by mixing calcium sulfate hemihydrate powders with pre-gelatinized starch powders using a mechanical blender, with proportions as described in Table 1. Each mixture was loaded into a three dimensional printing machine (Z400, Z Corporation) to print green specimens (80 mm × 10 mm × 4 mm) using layer thickness of 0.1 mm. Water-based binder was used as a jetting media in all formulations. After building, all the specimens were left in the machine for 2 h before removal and then left for drying in the laboratory for 24 h. The specimens were then air blown to remove any unbound powders. The cast plaster test material was prepared by mixing calcium sulfate hemihydrate with distilled water and pouring into the mould for setting reaction overnight. In the case of treatment in di-sodium hydrogen phosphate solution, 1 M of solution was prepared and all specimens were immersed in the solution and kept at 80°C for 4, 8, 16 and 24 h in the oven. After reaching the specified soaking periods, samples were taken out, rinsed by distilled water and oven dried.

2.3 Material characterizations

XRD characterization was carried out using a JEOL JDX 3530 X-ray diffractometer with Co K-alpha radiation in the range of 10–80° 2θ, a counting time of 0.5 second and a step angle of 0.02°. JCPDS files were used to identify the peaks of main components in sample. Functional groups in each sample were analyzed by Fourier transform infrared spectroscopy (Perkin Elmer Spectrum One) equipped with TGS detector. IR spectra were obtained over the region 400–4000 cm^{-1} using the KBr pellet technique with a resolution of 4 cm^{-1}. Flexural tests were performed on a universal testing machine (Instron 55R4502) equipped with a 10 kN load cell. All the tests were carried out at 23°C and 50% RH using three point bending method and a constant crosshead speed of 1.9 mm min^{-1}. Microstructures of the specimens were examined using a scanning electron microscope (JEOL JSM-5410) at an accelerating voltage of 20 kV. All samples were gold sputtered prior to the observation. Energy dispersive spectroscopy (EDS, Oxford Instruments) was employed to determine calcium and phosphorus elements in the sample.

Table 1 Materials formulation

Formulations	Calcium sulfate hemihydrate (%)	Pregelatinized starch (%)	Process
Plaster	100	0	Casting
3DP70	70	30	3DP
3DP85	85	15	3DP
3DP90	90	10	3DP

2.4 In vitro cell culture

Each sample was autoclaved at 121°C for 15 min prior to cell culture studies. Human osteoblast cells (h-OBs) at a density of 5 × 10^4 cells/ml were cultured on the sample in alpha-MEM supplemented with 10% fetal bovine serum and antibiotics in 95% air and 5% CO_2. The incubation periods used were 14 and 21 days. After reaching these periods, cultured samples were dried using ethanol and hexamethyldisilazane, gold sputtered and then observed by a scanning electron microscope (JEOL JSM-5410) at an accelerating voltage of 3 kV. Energy dispersive spectroscopy (EDS, Oxford Instruments) was also employed to determine the elements on the cell surfaces.

3 Results

3.1 Phase composition and functional group

Figure 1 shows the nature of as-fabricated 3DP samples after immersing in di-sodium hydrogen phosphate solution. As for cast plaster, the 3DP85 and 3DP90 samples were insoluble and could retain their integrities. In contrast, 3DP70 disintegrated immediately in a similar manner to the sample fabricated from commercial ZP100 powder. This ZP100 powder, available from 3DP machine manufacturers, consist of plaster material with numerous additives that maximize surface finish, feature resolution, and part strength, but it is not suitable for moist or liquid environment [20, 21]. Therefore, 3DP70 was discarded from further investigation. Figure 2 shows XRD patterns of unsoaked and soaked 3DP85 samples at different periods. It shows that calcium sulfate hemihydrate in 3DP sample almost completely

Fig. 1 Typical behavior of samples after soaking in solution

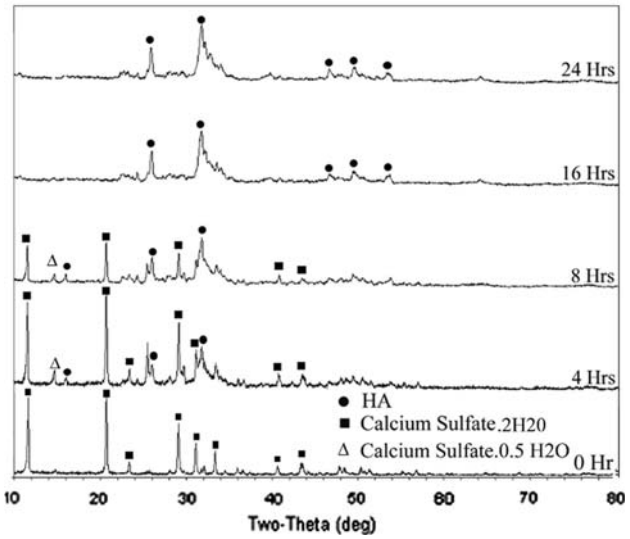

Fig. 2 XRD patterns of unsoaked and soaked 3DP85 samples at different periods

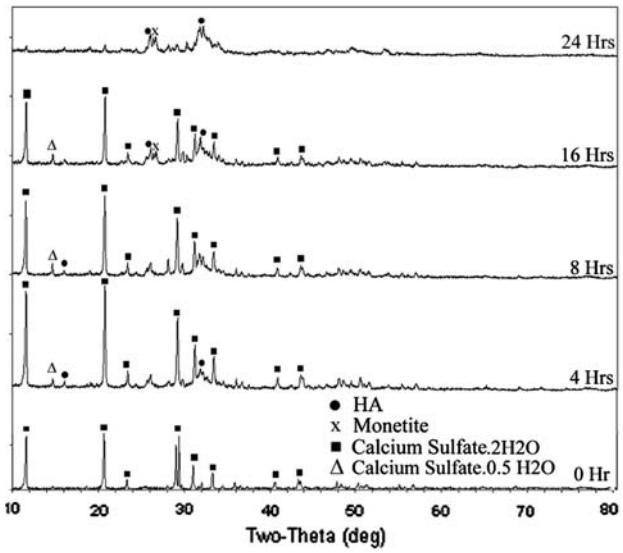

Fig. 3 XRD patterns of unsoaked and soaked 3DP90 samples at different periods

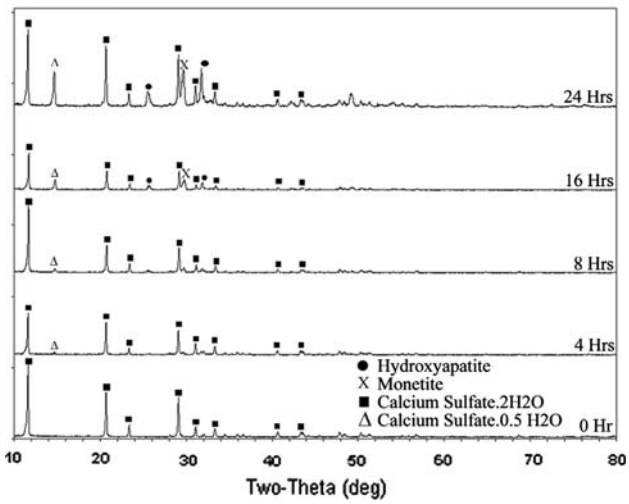

Fig. 4 XRD patterns of unsoaked and soaked plaster samples at different periods

transforms to calcium sulfate dihydrate during the three dimensionally printing process. At 4 h soaking, it can be seen that hydroxyapatite phase starts to appear and coexists with calcium sulfate dihydrate. It can also be noted that some calcium sulfate dihydrate changes back to calcium sulfate hemihydrate. At 8 h soaking, calcium sulfate dihydrate peaks can still be seen, but their intensity is lower than for 4 h. In contrast, the intensity of hydroxyapatite peaks increases. At 16 h, limited calcium sulfate peaks are observed, but these completely disappear at 24 h and all major peaks can be attributed to hydroxyapatite. In the case of 3DP90 (Fig. 3) the general transformation process is similar to 3DP85 except that nearly complete conversion to calcium phosphate needs 24 h and monetite also occurs in addition to hydroxyapatite. Figure 4 shows XRD patterns of cast plaster as a control sample. After soaking, cast plaster changes to calcium sulfate hemihydrate, hydroxyapatite and monetite. However, rate of transformation is much lower in comparison to the 3DP samples. Even at 24 h, incomplete transformation is observed in the cast plaster material. Figures 5 and 6 show infrared spectrum of unsoaked and soaked 3DP samples. Both unsoaked 3DP85 and 3DP90 show characteristic bands of calcium sulfate dihydrate including 602 and 669 cm^{-1} (υ_4 $(SO_4)^{2-}$ bending vibration), 1119 and 1142 cm^{-1} (υ_3 $(SO_4)^{2-}$ stretching vibration), 3544 and 3404 cm^{-1} (υ_3 and υ_1 H_2O stretching vibration), 1621 and 1685 cm^{-1} (υ_2 H_2O bending vibration). After soaking, both 3DP samples show the spectra bands similar to hydroxyapatite including 1028 and 1102 cm^{-1} (υ_3 PO_4^{3-} bending vibration), 1658 and 3403 cm^{-1} (adsorbed water), 561 and

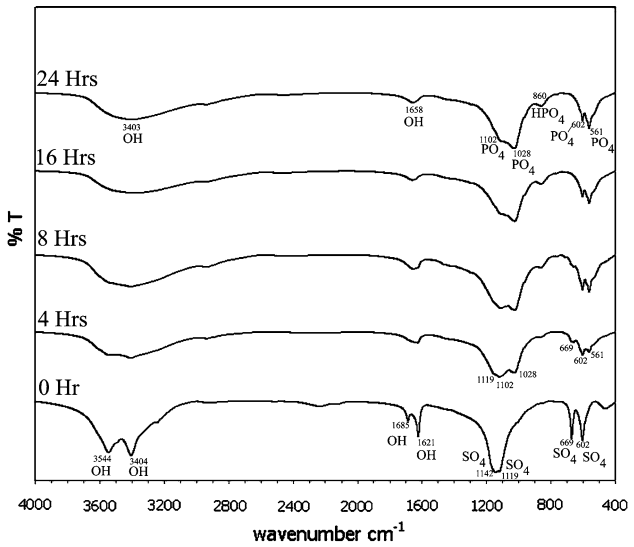

Fig. 5 IR spectrum of unsoaked and soaked 3DP85 samples at different periods

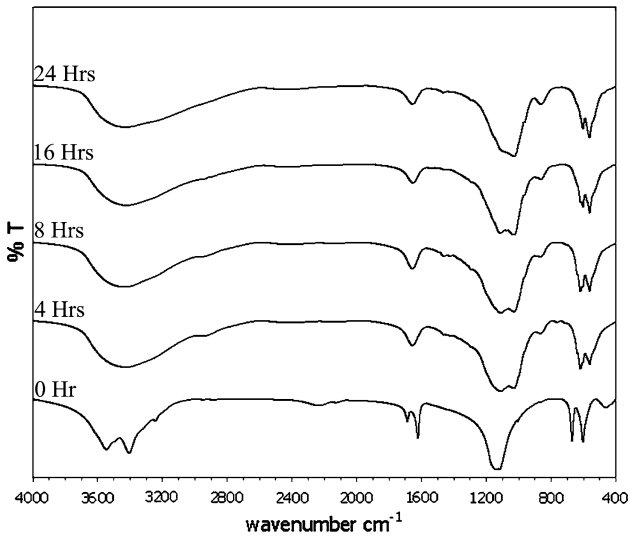

Fig. 6 IR spectrum of unsoaked and soaked 3DP90 samples at different periods

602 cm^{-1} (υ_4 PO_4^{3-} bending vibration), 860 cm^{-1} (HPO_4^{2-}). This HPO_4^{2-} may belong to monetite as detected by XRD in 3DP90 and cast plaster samples. However, this assigned band is also found for 3DP85 which contains only hydroxyapatite. Ca/P ratios, which were determined from EDS, were non-stoichiometric and in the range of 1.47–1.64 for 3DP85 and 1.14–1.82 for 3DP90. In addition, Na was also detected in all specimens. Therefore, the precipitated hydroxyapatite could be regarded as calcium deficient hydroxyapatite (CDHA) with substitution of Na^+ from the soaking solution. It should also be noted that the intensities of bands at 1119 and 602 cm^{-1} which are overlapped peaks of both SO_4^{2-} and PO_4^{3-} continuously decrease with increasing soaking time. This indicates the gradual change from calcium sulfate dihydrate to calcium phosphate.

3.2 Microstructure

Figure 7 shows the microstructures of un-soaked and soaked 3DP85 samples at various periods. Initially, the unsoaked sample is porous, comprising clusters of rod-like crystals forming the plate-like structure of calcium sulfate. After soaking in phosphate solution for 4 h, small needle-like crystals of hydroxyapatite are formed in addition to the plate-like crystals. Further increases in soaking time increases the amount of needle-like crystals. At 16 and 24 h, only the needle-like structure is seen in the samples and the increase in densification of structure is obviously seen. At similar soaking times between 4 and 16 h, the microstructure of the 3DP90 sample is denser than that of 3DP85, but it becomes more porous than that of 3DP85 at 24 h as shown in Fig. 8. Prior to soaking, plate-like and irregular shape structures are observed for 3DP90. Needle-like crystals are found to form after soaking in phosphate solution similarly to 3DP85 and the amount also increases with increasing soaking time. However, the proportion of needle-like crystals is lower than 3DP85 at similar soaking periods. It is only after 24 h soaking time that the needles are clearly seen throughout the sample. The microstructure of cast plaster is different from both 3DP samples as a result of different processing routes. It comprises a random entanglement of rod-like crystals throughout the sample (Fig. 9). After soaking, needle-like crystals are also formed, but the amount is much lower than in the 3DP samples and the needle size is also much smaller. The overall structure shows a higher density than 3DP.

3.3 Flexural properties

Figures 10 and 11 show the measured flexural modulus and strength of unsoaked and soaked samples after different soaking periods. Prior to soaking, cast plaster has the greatest modulus and strength followed by 3DP85 and 3DP90 respectively. After soaking, the modulus of cast plaster decreases significantly with increasing soaking time from about 6 to 3 GPa. In contrast, the modulus for both the 3DP samples increases slightly after soaking and values for 3DP85 are greater than for 3DP90 at all soaking times, ranging from about 1.5 to 1.8 GPa. In the case of strength, a decrease in the flexural strength was observed for the cast plaster and the 3DP90 samples after 4 h whilst an increase was observed with the 3DP85 samples. Beyond 4 h, the strength of the cast plaster remained constant until 16 h and then decreased again at 24 h to a similar value to that for 3DP90. The strength of 3DP85 slightly decreased further at 8 h and remained relatively unchanged up to 24 h. In

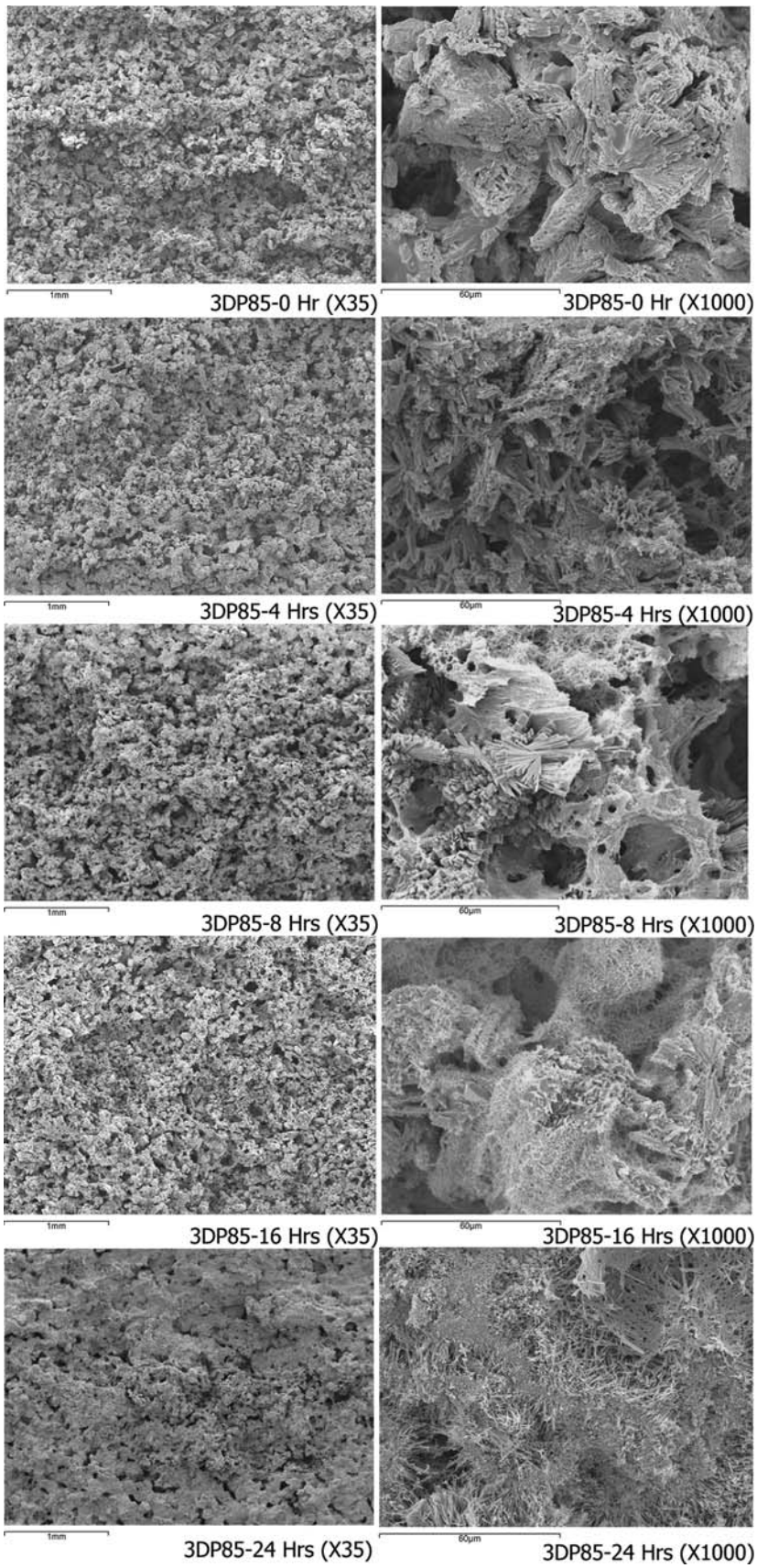

Fig. 7 Microstructure of unsoaked and soaked 3DP85 samples at different periods

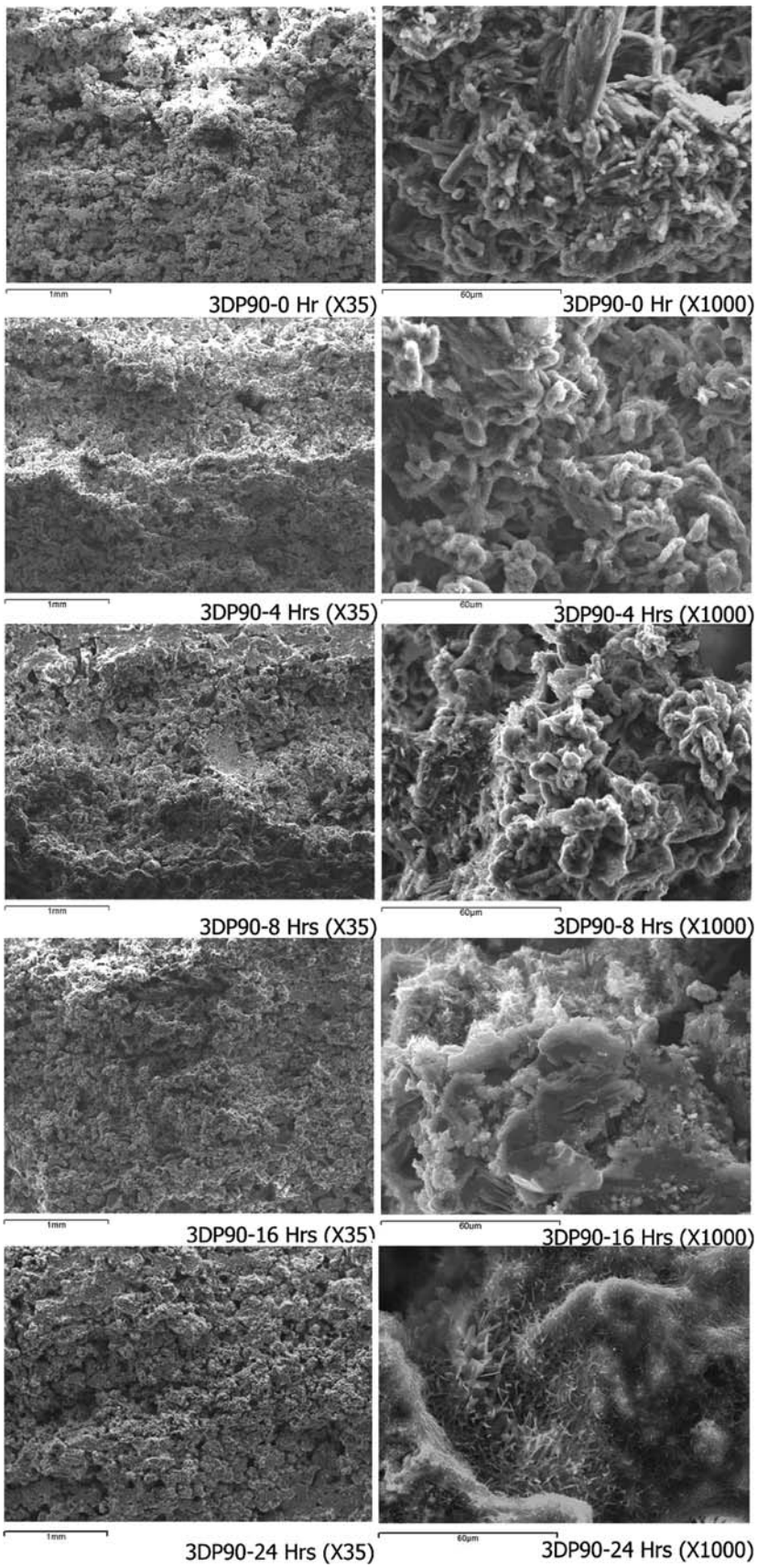

Fig. 8 Microstructure of unsoaked and soaked 3DP90 samples at different periods

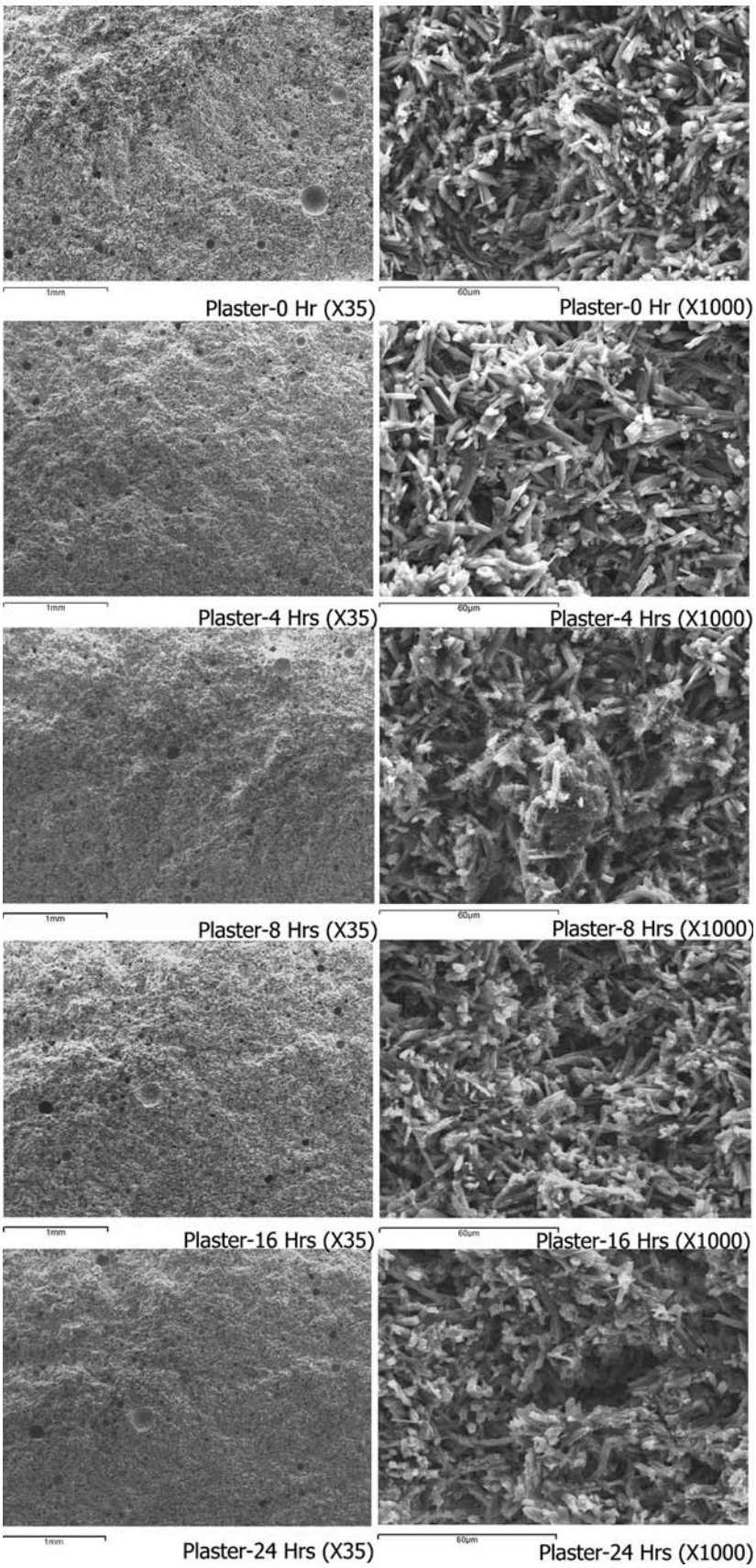

Fig. 9 Microstructure of unsoaked and soaked plaster samples at different periods

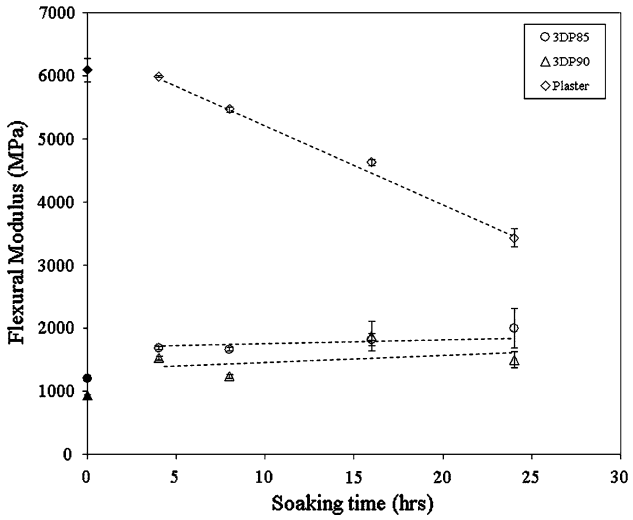

Fig. 10 Changes in flexural modulus of plaster and 3DP samples after soaking in phosphate solution at different periods

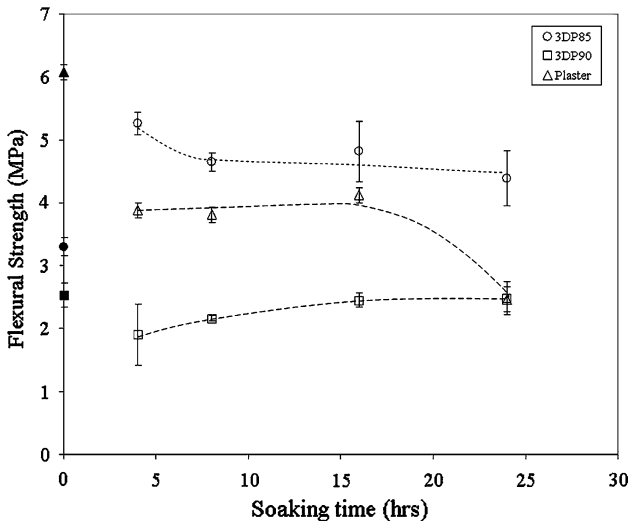

Fig. 11 Changes in flexural strength of plaster and 3DP samples after soaking in phosphate solution at different periods

contrast, the strength of 3DP90 slightly increased with further increases in soaking time.

3.4 Cell culture

Figure 12 shows the scanning electron microscope images of human osteoblast cells cultured for 14 and 21 days on the surface of the 3DP85 sample. It can be seen that cells spread, adhere and attain a normal morphology on surfaces of this sample. Many cell filipodia extending from cell bodies are also observed. At day 21, three-dimensional mineralized nodule formation is also observed. EDS analysis on the cell confirms the presence of calcium.

4 Discussion

A combination of the 3DP manufacturing process with phase transformation provides the potential to easily direct fabricate customized calcium phosphate scaffold or bone replacement parts having desirable external and internal geometries without employing a high temperature sintering operation. Previously, Lowmunkong et al. showed that this concept was possible, but the resulting structure was fragile and not suitable for practical use since heat treatment at 300°C was needed to make the 3DP specimens insoluble in solution. This present study shows the development of calcium sulfate hemihydrate based formulations as raw materials for the 3DP process which after printing can be directly soaked in phosphate solution without the need for heat treatment. Pregelatinized starch was selected as the adhesive binder in this processing step and to help in stabilizing the structure during soaking in solution since it is inexpensive and provides sufficient bonding strength. However, it should be used in amounts no greater than 30%. Otherwise, the amount of calcium sulfate hemihydrate is too low to hold the structure together while soaking in phosphate solution. Different formulations and process were observed to affect the phase transformation and properties of the produced parts. Both 3DP samples transformed to calcium phosphate much faster than the cast plaster. After 24 h soaking period, considerable incomplete conversion was seen for cast plaster while the 3DP85 and 3DP90 completed or nearly completed conversion to calcium phosphate. The difference in transformation rate is believed to be mainly due to the difference in porosity of the samples. In the phase transformation process, calcium sulfate dihydrate would slightly dissolve when contacting phosphate solution and release calcium and sulfate ions which could combine with phosphate ions in the solution to form calcium phosphate crystals as shown in Eqs 1 and 2.

$$\mathrm{CaSO_4 \cdot 0.5\ H_2O} \xrightarrow{\mathrm{3DP}} \mathrm{CaSO_4 \cdot 2H_20} \xrightarrow{\mathrm{Na_2HPO_4}} \mathrm{Ca^{2+}} + \mathrm{SO_4^{2-}} + \mathrm{2H_2O} + \mathrm{HPO_4^{2-}} + \mathrm{2Na^{+}} \quad (1)$$

$$\mathrm{10Ca^{2+} + 4SO_4^{2-} + 2H_2O + 6HPO_4^{2-}} \rightarrow \mathrm{Ca_{10-x}(HPO_4)_x(PO_4)_{6-x}(OH)_{2-x} + 4H_2SO_4} \quad (2)$$

Therefore, this transformation would start from the outermost surface and gradually advance into the inner part of the sample with time. An increase in porosity increases the diffusion rate and amount of phosphate solution which can penetrate and exchange ions with the sample. From microstructural observation of unsoaked material in Figs. 7 and 9, it can be seen that cast plaster has the densest structure following by 3DP90 and 3DP85. The porous structure of both 3DP samples is the result of using organic binder to fast set the layered sample during the 3DP

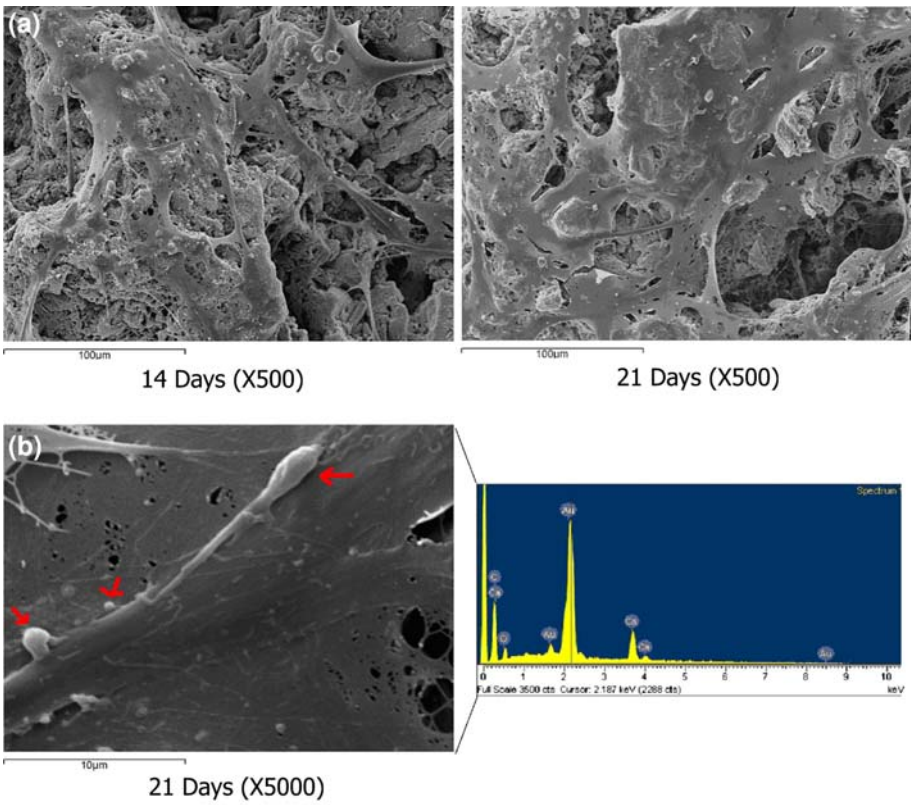

Fig. 12 **a** Behavior of osteoblast cells on surface of 3DP85 sample at 14 and 21 days incubation periods (×500). **b** EDS spectrum on the surface of the osteoblast cell. *Arrows* indicate nodule structures (×5000)

process. This binder can be an obstacle for crystal formation and leaches out during soaking. The increase in binder content increased the porosity and this correlated well with the level of transformation rate as discussed.

The 3DP85 sample transformed to calcium deficient hydroxyapatite (CDHA) while a mixture of CDHA and monetite was formed for 3DP90 and cast plaster. As the reaction proceeds, sulfate ion is released continuously causing the pH of the solution to decrease from its initial value of 10 to about 7 after 24 h. Since the precipitation of calcium phosphate in this reaction is based on the difference in thermodynamic stability amongst different types of calcium phosphate and it was reported that the CDHA phase was stable at pH 6.5–9.5 while monetite phase was stable at pH 2.0–6.0 and at temperatures greater than 50–80°C [11], a decrease in pH of the solution with soaking time would cause hydroxyapatite to become unstable in comparison to monetite. Since 3DP85 has the lowest amount of calcium sulfate and greatest porosity, this may produce a favorable basic environment sufficient for hydroxyapatite precipitation whereas the higher amount of calcium sulfate and the lower porosity in 3DP90 and in cast plaster may cause a localized decrease in pH especially at the inner area where lower amount of solution can reach. Co-precipitation of monetite thus occurs. In addition, XRD analysis of material collected from the surface and inner core of both samples also confirms that monetite was found only at the inner core area, but not at the surface.

Mechanical properties of the samples were found to vary with material formulation and soaking periods. It was reported previously that the mechanical properties of gypsum or mixed gypsum would decrease after transformation by soaking in phosphate solution [17, 18]. In this study, cast plaster does show a large and continuous drop in modulus with increasing soaking times. In contrast, both 3DP85 and 3DP90 show an increase in modulus after soaking. This is possibly due to the reinforcing effect of newly formed calcium phosphate crystals with the initial calcium sulfate crystals since the unsoaked 3DP samples were relatively porous. Calcium phosphate crystals can form both on calcium sulfate crystals and can grow into the pores amongst the cluster of initial crystals producing a denser structure with time as shown in SEM images in Figs. 7 and 8. In the case of cast plaster, calcium phosphate crystals would form primarily on the original calcium sulfate crystals themselves. No reinforcement effect occurs, but the replacement of crystal entanglement of long and large rod-like calcium sulfate by short and small needle-shaped crystal is responsible for the decrease in modulus. In the case of strength, 3DP85 showed the greatest strength at all soaking periods. However, a slight decrease in strength with soaking times beyond 4 h may be caused

by the reduction of reinforcement efficiency by an increase in the amount of lower strength needle-like apatite crystals. In contrast, a continuous decrease in the strength of cast plaster with soaking time was observed and could be explained similarly as in the case of the modulus value. These levels of strength were found to be equal or even greater than other 3DP calcium phosphates which used calcium phosphate cement chemistry [9, 12, 15, 16]. However, those studies employed a solution of phosphoric acid or sodium phosphate as jetting binders. This may affect the performance and long-term stability of the printhead and other related components since these components were not designed to work with those solutions. In contrast, this work attempted to modify only the powders formulation such that the working of the printing machine was not affected. Although this approach needs an additional post-processing step for conversion which seems to be a drawback, additional post-hardening and post-phase transformation also had to be employed in those studies if increased strength or specified amount of calcium phosphate phase were required. In addition, the type of the resultant calcium phosphate phase is easier to control in this present study.

As 3DP85 shows the faster rate of transformation and higher mechanical properties, it was selected for further cell culture study to observe the response of material to human osteoblast cells. Preliminary cell culture shows that the 3DP85 is non-toxic to osteoblast cells. The cells spread, adhere and attain a normal morphology on surfaces of this material and mineralized nodules of various size and shapes were also observed. Mineralized nodule formation is basically considered to be the final result of differentiation and function of the osteoblasts [22, 23]. Thus, this cell culture result proves that 3DP85 can potentially be used as a scaffold and bone replacement material. However, further investigation on both in vitro and in vivo performance is needed to confirm the applicability of this new material. In order to illustrate the intended application of the process developed, Fig. 13 shows a bone implant which was fabricated by 3DP85 intended for skull defect reconstruction. This model went through all processing steps successfully and the final implant fits well with the defect contour. This would be beneficial for patients who require individual implant customization.

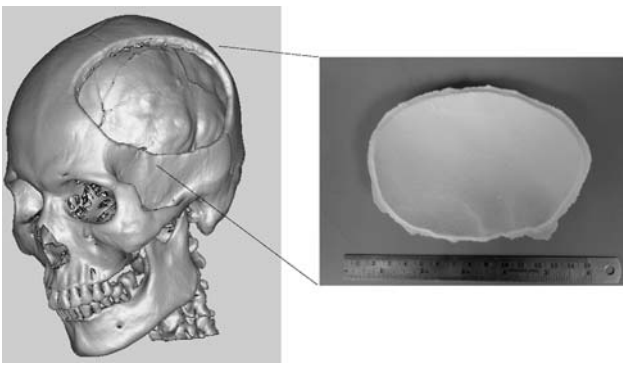

Fig. 13 Hydroxyapatite skull implant made of transformed 3DP85 sample

5 Conclusion

Low crystalline calcium phosphates including monetite and calcium deficient hydroxyapatite were successfully fabricated by phosphorization of three dimensionally printed calcium sulfate hemihydrate based materials at low temperature. Transformation rate, phase composition and mechanical properties were influenced by differences in porosity in the samples resulting from difference in materials formulation and soaking times. The composition which gave the fastest transformation rate and greatest mechanical properties comprised 85% $CaSO_4 \cdot 0.5\ H_2O$ and 15% pregelatinized starch. The advantage of this fabrication technique is that the structure can be tailor made to fit the required shape and size with virtually no limitation.

Acknowledgment This work was supported by a grant from National Metal and Materials Technology Center, National Science and Technology Development Agency. The authors would like to extend their gratitude to R. Sanngam and J. Jaresitthikulchai for helping in SEM and cell culture work, respectively.

Referencess

1. Chumnanklang R, Panyathammaporn T, Sitthiseripratip K, Suwanprateeb J. 3D printing of hydroxyapatite: effect of binder concentration in pre-coated particle on part strength. Mater Sci Eng C. 2007;27:914–21.
2. Simon JL, Roy TD, Parsons JR, Rekow ED, Thompson VP, Kemnitzer J, et al. Engineered cellular response to scaffold architecture in a rabbit trephine defect. J Biomed Mater Res. 2003;66A:275–82.
3. Roy TD, Simon JL, Ricci JL, Rekow ED, Thompson VP, Parsons JR. Performance of hydroxyapatite bone repair scaffolds created via three-dimensional fabrication techniques. J Biomed Mater Res. 2003;67A:1228–37.
4. Seitz H, Rieder W, Irsen S, Leukers B, Tille C. Three-dimensional printing of porous ceramic scaffolds for bone tissue engineering. J Biomed Mater Res Part B: Appl Biomater. 2005;74B:782–8.
5. Will J, Melcher R, Treul C, Travitzky N, Kneser U, Polykandriotis E, et al. Porous ceramic bone scaffolds for vascularized bone tissue regeneration. J Mater Sci: Mater Med. 2008;19:2781–90.
6. Suwanprateeb J, Sanngam R, Suwanpreuk W. Fabrication of bioactive hydroxyapatite/bis-GMA based composite via three dimensional printing. J Mater Sci: Mater Med. 2008;19:2637–45.
7. Suwanprateeb J, Sanngam R, Suvannapruk W, Panyathanmaporn T. Mechanical and in vitro performance of apatite–wollastonite

glass ceramic reinforced hydroxyapatite composite fabricated by 3D-printing. J Mater Sci: Mater Med. 2009;20:1281–9.
8. Khalyfa A, Vogt S, Weisser J, Grimm G, Rechtenbach A, Meyer W, et al. Development of a new calcium phosphate powder-binder system for the 3D printing of patient specific implants. J Mater Sci: Mater Med. 2007;18:909–16.
9. Szucs TD, Brabazon D. Effect of saturation and post processing on 3D printed calcium phosphate scaffolds. Key Eng Mater. 2009;396–398:663–6.
10. Benhayoune H, Jallot E, Laquerriere P, Balossier G, Bonhomme P, Frayssinet P. Integration of dense HA rods into cortical bone. Biomaterials. 2000;21(3):235–42.
11. Dorozhkin SV. Calcium orthophosphates. J Mater Sci. 2007;42: 1061–5.
12. Gbureck U, Holzel T, Biermann I, Barralet JE. Preparation of tricalcium phosphate/calcium pyrophosphate structures via rapid prototyping. J Mater Sci: Mater Med. 2008;19:1559–63.
13. Varndran E, Klarner M, Klammert U, Grover LM, Patel S, Barralet JE, et al. 3D powder printing of -tricalcium phosphate ceramics using different strategies. Adv Eng Mater. 2008;10: B67–71.
14. Igawa K, Mochizuki M, Sugimori O, Shimizu K, Yamazawa K, Kawaguchi H, et al. Tailor-made tricalcium phosphate bone implant directly fabricated by a three-dimensional ink-jet printer. J Artif Organs. 2006;9:234–40.
15. Gbureck U, Holzel T, Doillon CJ, Muller FA, Barralet JE. Direct printing of bioceramic implants with spatially localized angiogenic factors. Adv Mater. 2007;19:795–800.
16. Gbureck U, Holzel T, Klammert U, Wurzler K, Muller FA, Barralet JE. Resorbable dicalcium phosphate bone substitutes prepared by 3D powder printing. Adv Funct Mater. 2007;17: 3940–5.
17. Zaman CT, Takauchi A, Matsuya S, Zaman QHMS, Ishikawa K K. Abrication of B-type carbonate apatite blocks by the phosphorization of free-molding gypsum-calcite composite. Dent Mater J. 2008;27(5):710–5.
18. Ishikawa K, Suzuki Y, Matsuya S, Nakagawa M, Koyano K. Effects of pH on the transformation of gypsum to carbonate apatite in the presence of ammonium hydrogen phosphate. Key Eng Mater. 2006;309–311:199–202.
19. Furuta S, Katsuki H, Komarneni S. Porous hydroxyapatite monoliths from gypsum waste. J Mater Chem. 1998;8:2803–6.
20. Lowmunkong R, Sohmura T, Takahashi J, Suzuki Y, Matsuya S, Ishikawa K. Transformation of 3DP gypsum model to HA by treating in ammonium phosphate solution. J Biomed Mater Res Part B: Appl Biomater. 2007;80B:386–93.
21. Suwanprateeb J. Comparative study of 3DP material systems for moisture resistance applications. Rapid Prototyping J. 2007;13(1): 48–52.
22. Zhou Z, Chen L. Morphology expression and proliferation of human osteoblasts on bioactive glass scaffolds. Mater Sci -Poland. 2008;26(3):506–16.
23. Dastjerdi MN. Induction of mineralized nodule formation in rat bone marrow stromal cell cultures by silk fibroin. Iran Biomed J. 2006;10(3):133–8.